A migration based reconstruction algorithm for the imaging of defects in a plate using a compact array

Ajith Muralidharan*, Krishnan Balasubramaniam‡ and C.V. Krishnamurthy‡†

*Center for Nondestructive Evaluation, Department of Mechanical Engineering,
Indian Institute of Technology, Madras, Chennai-600036, India*

Abstract.   An array based, outward monitoring, ultrasonic guided wave based SHM technique using a single transmitter and multiple receivers (STMR), with a small footprint is discussed here. The previous implementation of such SHM arrays used a phase-reconstruction algorithm (that is similar to the beam-steering algorithm) for the imaging of reflectors. These algorithms were found to have a limitation during the imaging of defects/reflectors that are present in the "near-field" of the array. Here, the "near-field" is defined to be approximately 3-4 times the diameter of the compact array. This limitation is caused by approximations in the beam-steering reconstruction algorithm. In this paper, a migration-based reconstruction algorithm, with dispersion correction in the frequency domain, is discussed. Simulation and experimental studies are used to demonstrate that this algorithm improves the reconstruction in the "near-field", without decreasing the ability to reconstruct defects in the "far-field" in both isotropic and anisotropic plates.

Keywords: migration; STMR array; ultrasonic guided waves; SHM.

1. Introduction

Structural Health Monitoring (SHM) is an emerging field due to its vast potential for building-in reliability and safety into the structure as well as for reducing the maintenance overheads. It involves monitoring the changes in a structure with attached/embedded sensors, and processing the acquired data to arrive at life cycle management decisions. The applications of SHM range from ship and aircraft industries to civil structures (Boller 2000, Fujino and Abe 2004).

Plate like structures find a variety of uses ranging from panels in aircrafts to oil storage tanks. During service, these structures are subjected to corrosion and fatigue cracks, in addition to other forms of damage. Monitoring of these structures using conventional methods of NDE is expensive and time consuming. Also, in many cases, the cost of these inspections is difficult to justify, given that many of the NDT inspections do not reveal any defects that may potentially cause catastrophic damage. The inspection of these structures has been recently supplemented using techniques that employ guided ultrasonic waves. Guided ultrasonic waves in plates are often known as Lamb waves. These waves are guided by the boundaries of the plate structure and can travel long distances, thereby making it suitable

*Student, E-mail: ajithm@gmail.com
‡Professor, E-mail: balas@iitm.ac.in
‡†Principal Project Officer, E-mail: cvkmind@gmail.com

for large area structural health monitoring (SHM). Lamb waves are multi-modal and these modes can be dispersive i.e., the wave velocity varies with frequency-thickness product (Victorov 1967, Rose 1999). Signal processing for dispersion correction have been developed (Wilcox, *et al.* 2000, Sicard, *et al.* 2002). Much of the research work carried out focuses on using only a single guided wave mode and measures are taken to minimize the number of modes that are generated in the plate, by working at lower frequencies and sometimes by also using angular excitation.

One of the methods for implementation of the guided wave inspection would be the use of Multiple Transmitters and Multiple Receivers (MTMR) Array that can monitor a pre-determined area in the plate-like structure. The data is collected and the damage state of the monitored area is 2-dimensionally imaged using tomography techniques (Malyarenko and Hinders 2001). Iterative tomography techniques have been popular for image reconstruction (Subbarao, *et al.* 1996) due to the limited data sets that can be obtained. SHM using such methods have been shown on isotropic (Giurgiutiu and Zagrai 2002) and in anisotropic plates (Prasad, *et al.* 2003, Prasad, *et al.* 2003b, Jagannathan, *et al.* 2004).

Data reconstruction techniques like Kirchoff Migration (similar to the Synthetic Aperture Focusing Technique (SAFT) that is used in the fields of NDT and Radar) have successfully helped in imaging various features in seismology, and geophysics. Initially, a re-construction technique by Hagedoorn (Fehler and Huang 2002, Bleistein and Gray 2001) that consisted of finding reflectors on equal timeline curves defined by events on a seismic trace was introduced in the field of seismic imaging. This technique consisted of draw equal timeline traces using compass and locating the defects. Kirchoff migration was later developed and widely used in imaging seismic data. Connection between Hagedoorns' technique, Kirchoff migration and Kirchoff inversion has been investigated recently (Bleistein and Gray 2001). SAFT usage in NDT followed from its usage in the field of radar (Prine 1972). SAFT has inherent advantages like better signal to noise ratio, and quick reconstruction of large area. Also, it is better compared to conventional B-Scans (Seydel 1982, Schmitz, *et al.* 2000) as it attempts to nullify beam spreading. Guided waves as well as bulk waves have been imaged using SAFT algorithms like F- SAFT (SAFT in the frequency domain) and L-SAFT (Lamb-SAFT to correct for dispersion in plates) (Sicard, *et al.* 2002). SAFT based algorithms have also been used for defect reconstruction in anisotropic media (Spies and Jager 2003). SAFT based techniques were also developed for isotropic plate's dispersion correction to eliminate the effects of dispersion while scanning the plate using a linear aperture, thereby reducing the time of inspection (Wilcox, *et al.* 1999, Sicard, *et al.* 2002).

It must be noted here that it is customary to define SAFT as a technique where a single transmitter/ receiver combination is employed and this is either translated and/or rotated to obtain multiple data sets. Here, the transmitter and the receivers are often co-located. However, for SHM applications, the movement of the probes is not desirable, and hence, arrays of transmitters and/or receivers are used. This allows for the migration based algorithms to be used in a more Complete-Matrix approach. When both the transmitter and the receivers arrays are used, it leads to a Multi Transmitter Multi Receiver (MTMR) configuration (also called as Full Matrix or Total Focusing Method or Sampled Array Technique, Davies and Cawley 2006). The STMR technique discussed here only uses a receiver array and hence is a Partial-Matrix method and sometimes has also been called as Common Source Method.

The use of the Migration/SAFT based Algorithms for the Structural Health Monitoring (SHM) using Lamb waves that are generated and received by transducer arrays have been reported for quick inspection of large plates-like structures (Wilcox 2002). The applicability of an electromagnetic acoustic transducer (EMAT) array based system, consisting of multi transmitters and multi receivers (MTMR), for rapid inspection of large plate structures, found in storage tank floors, using a beam steering algorithm was demonstrated. It has also been shown that the use of MTMR in a phased manner provides
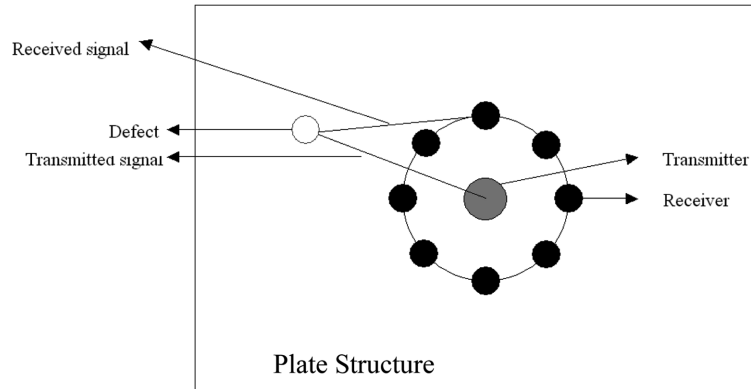
Fig. 1 The STMR compact array configuration

improved transduction and increases the area of coverage (Wilcox 2003). In these cases, circular arrays have been used for rapid inspection throughout the plate geometry. These arrays make use of the fact that waves propagating are two-dimensional, and can yield information in all the directions. Also the data collected by an omni-directional receiver like a piezoelectric crystal contains information of all reflectors in all the directions. By collecting data using from the array of receivers, one can use phase shifting and addition to determine the location of reflecting features. This forms the basis of the reconstruction algorithms that have been used. The advantage of circular array is that using the data obtained we can obtain reconstruction similar to a linear array being rotated, whereas there is no 'physical' rotation of the receivers. Thereby one can image the whole structure from a set of sensors fixed at a single location.

Here, a Single Transmitter Multiple Receiver compact array system (STMR) was used (Rajagopalan, *et al.* 2006) as illustrated in Fig. 1. A single PZT transducer element was employed to excite ultrasonic guided waves in the plate. The transducer is expected to excite omni-directional waves. The type of crystal used for the wave generation will depend on the guided wave mode type that is to be generated (either the fundamental symmetric or anti-symmetric mode). The transmitter is surrounded by several receiver elements that receive the direct signals (as the wave propagates beneath the receivers) as well as reflected signals from defects and geometric discontinuities in the plate like structure. The first received direct signal was used to normalize the amplitude and arrival times of the reflected waves from defects/reflectors. This was done mainly to normalize the amplitudes which may vary due to coupling variations. The time of flight (arrival time) is normally considered to a reliable feature that may not need normalization, once the velocities in the material are known. The direct received signals may also allow for the calculation of the velocity profiles in anisotropic materials. The receivers are arranged in a circle of diameter 'D' while the transmitter is placed at its center as shown in Fig. 1. A polar coordinate system is defined with its origin at the center of the array coinciding with the transmitter position. The positions of the receivers are defined using their radial and angular coordinates. The use of a single transmitter ensures uniform coverage. It also simplifies the task of data collection considerably as only the receivers are to be "arrayed. The parameters governing the image reconstruction therefore are the diameter of the circular array, D, the number of receivers, N, the sampled time difference, and the discretization element size of the domain during reconstruction computation. For carrying out simulations, the transmitter and the receivers are assumed to act as point sources and are considered to have equal transmission and reception sensitivity in all directions. Experiments were carried out with

conventional PZT crystals and the simulated results were well validated justifying the point source/ receiver assumption made in the simulations. It must be noted here that the STMR technique does not "steer the beam (as reported in Wilcox, *et al.* 1999), but instead the spatial resolution in the image is achieve by the phased addition reconstruction algorithm.

The implementation of the STMR for guided ultrasonic wave based SHM of isotropic and anisotropic plates has been earlier reported (Rajagopalan, *et al.* 2006) using a phased addition algorithm that is similar to the beam steering algorithm used by Wilcox, *et al*. However, this algorithm has a limitation while imaging defects and reflectors in regions near the compact array. Here, the "near-field" is defined to be approximately 3-4 times the diameter of the compact array configuration that includes the transmitter as well as the receivers.

This paper proposes to eliminate the deficiencies of the previously reported phased addition algorithm by eliminating approximation that causes poor image reconstruction the "near-field" region due to assumptions made in the algorithm. The first part describes the array structure and data acquisition, while the second part deals with the algorithm itself. A few simulation studies are shown to highlight the capabilities of the algorithm, and the reconstructed images are compared with the "far-field" approximated phased addition algorithm. Afterwards a parameter study was undertaken to determine the performance variation with different parameters of the array that emphasized the need for the proposed algorithm. Finally experiments are carried out to confirm the improvement in imaging using of the proposed "near-field" corrected migration based algorithm.

2. Array description and data acquisition

The array system considered for simulations and experiments is the STMR (single transmitter multiple receiver) system with omni-directional transducers. The STMR system has some desirable advantages over the MTMR (multiple transmitter multiple receiver) system used by Wilcox et al. such as reduced side lobe formation, relatively smaller footprint and the simpler electronics. It is preferred over the circular filled aperture as it has a similar performance with lesser number of elements. The array consists of an omni-directional transmitter fixed at the centre and receivers spread uniformly around a circle. Spatial aliasing is avoided by limiting the inter-element spacing to a maximum of half of the minimum wavelength, within the frequency range of excited guided waves. If this criterion is not adhered to, then false alarms may be triggered due to the grating lobes. The position of the array elements are defined in the polar co-ordinate system with the transmitter in the centre and the receivers spread equi-angularly along a circle of diameter D. It is assumed that the array elements behave like point sources.

The transmitter was excited and time domain signals were collected at the receivers and digitized using an *A/D* converter (National Instruments USB 5102). The acquisition and transformation of data begins with the acquisition of the raw data set in the uniformly sampled discrete time, $t(n)$, domain. The transmitter is excited and a discretely sampled time domain signal t is collected at each of the receivers. This data is used to form a matrix, **T**, in which each column represents the raw t domain signal collected at each of the 'N' receivers. Consequently, the number of columns in the **T** matrix is equal to the number of receivers. It is assumed that the range of frequencies of excitation is below the Nyquist frequency (half the sampling frequency).

This time domain data can be directly processed to obtain defect location data using conventional migration based procedures, if the velocity was constant with frequency. However, in the case of Lamb

waves in plate structures, due to dispersion, the phase velocity depends on frequency and hence this time data will not directly represent uniformly spaced data in the wave-number domain. This means that the Fourier transform of the received signals will produce equally spaced frequency spectrum while this will be a non-uniformly spaced wave-number domain data because the relation $k = \omega/v_{ph}$ (where v_{ph} is the phase velocity) leads to non-uniform spacing in the wave-number domain. Due to this if the data is processed assuming a constant "representative" velocity, it leads to errors in the image reconstruction, especially at highly dispersive regions. Thus all conventional processing for Lamb wave reconstruction needs to be done in wave-number domain (which is interpolated from frequency domain data) taking into account the velocity variation with frequency. In the present case the processing is done in the frequency domain itself, taking note of velocity at different frequencies. Thus the matrix **T** is subjected to a column wise Fast Fourier Transform (FFT) to get a matrix **S** in the complex frequency domain and this data is used for further processing. The advantage of processing in the frequency domain itself is that there is no need for interpolation which might introduce errors in the data.

3. Reconstruction algorithm

The phased addition reconstruction algorithm maps the positions of the reflectors (edges, defects and other discontinuities) in the area which is scanned. Omni-directional nature of the transmitter and its position in the centre of the array ensures uniform insonification along all directions. The domain of imaging is discretized in the **R-θ** coordinates and phased addition reconstruction is done pixel wise. For each pixel, the defect is assumed to be located at its centre, then the received signals are back-shifted to the point it was transmitted and then added. Ideally if the defect/reflector is located at the pixel considered, then the phased addition will be constructive and the resultant signal will resemble the transmitted signal. At any other point, where there is no reflector, the addition is less constructive, which will diminish the phase added amplitude for the point. As a result the signal to noise ratio is significantly improved. The location of the reflectors is then obtained by plotting the phase added intensity obtained at each point in a polar plot.

The image reconstruction domain is divided into N_1 equi-spaced angles and N_2 equi spaced radii. For each pixel, a reflector is assumed to be present at that location and the actual distances traveled by the
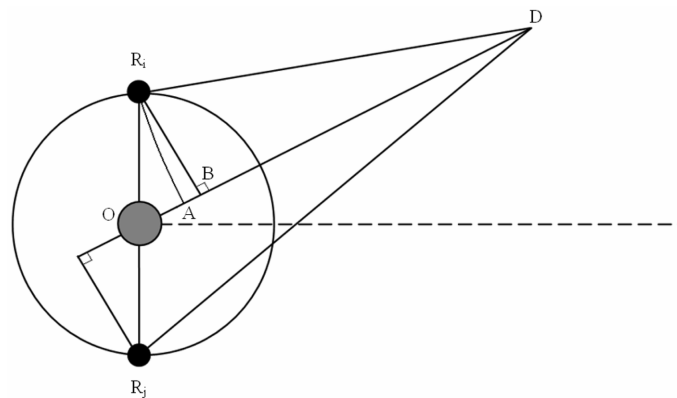

Fig. 2 Schematic representation of the STMR compact array based phase addition algorithms. Here only two receivers (R) are shown

wave from the transmitter to the receivers, after reflection from the reflector is calculated. As illustrated in Fig. 2, this distance is $OD+DR_i$, assuming that the pixel considered is D, and the receiver is R_i. The signals are time reversed in the frequency domain by the calculated time of flight and then added. Let $S_j(f)$ denote the spectra at frequency f of the acquired time domain signal from the receiver j. $A_{(r,\theta)}(f)$, which denotes the element corresponding to frequency f in the vector $\mathbf{A}_{(r,\theta)}$ (the spectra of the phase added signal for the pixel D with coordinates (r, θ)), is given by

$$A_{(r,\theta)}(f) = \sum_j S_j(f) \times \exp(i2\pi f t_j) \tag{1}$$

$$t_j = OD/v_{1_f} + DR_j/v_{2_f} \tag{2}$$

t_j refers to the time of flight of the wave from transmitter to the receiver j after reflection from the pixel D. Here v_{1f} denotes the velocity in the direction of OD which is same for all the terms of the summation. However v_{2f} which denotes the velocity in the direction of DR_j depends on the position of receiver, in the case of anisotropic media. These velocities are a function of frequency (f) and can be obtained from dispersion data of the guided wave mode chosen for reconstruction. Now $\mathbf{A}_{(r,\theta)}$ is subjected to an Inverse Fast Fourier Transform to give the back propagated and phase added signal $\mathbf{B}_{(r,\theta)}$. This is compared with the transmitted signal by noting the amplitude of the reconstructed signal at the time when the transmitted signal has a peak. This value is taken to be representative of probability of reflector location at that point, which will have large amplitude when a reflector is actually located at that point. Thus the elements of the reconstructed output matrix is given by

$$O(r, \theta) = B_{(r,\theta)}(t_{peak}) \tag{3}$$

where t_{peak} represents the time corresponding to the peak in the transmitted signal. Each row in $\boldsymbol{O}$ corresponds to a particular radius, while each column corresponds to a particular angle. This is plotted in a logarithmic scale (dB Scale) to obtain the reconstructed image. The procedure followed has been summed up in Fig. 3.

The algorithm described in this paper is based on the migration algorithm, where the signals are time reversed and added to provide synthetic focusing in the reflector positions. In comparison, the previous "far-field" algorithms (Rajagopalan, *et al.* 2006, Rajagopalan, *et al.* 2006, Wilcox 2003) are based on beam steering, which is effected by applying phase shifts to the received signals and then adding them. The beam steering phase factors are calculated for each direction and the image is reconstructed. To calculate the steering factors for each direction, these algorithms approximate the distance from the pixel to the receiver by the perpendicular projection of this distance on the radial line joining the

$$T(t) = [\ T_1\ T_2\ \dots\ T_n\ ] \xrightarrow{\ \ \ FFT\ \ \ } S(f) = [S_1\ S_2\ \dots S_n]$$

Phased addition for all (r,θ)

$$O(r,\theta) = B_{(r,\theta)}(t_{peak}) \xleftarrow{\text{Reconstructed Intensity map}} B_{(r,\theta)} \xleftarrow{\ \ IFFT\ \ } A_{(r,\theta)}$$
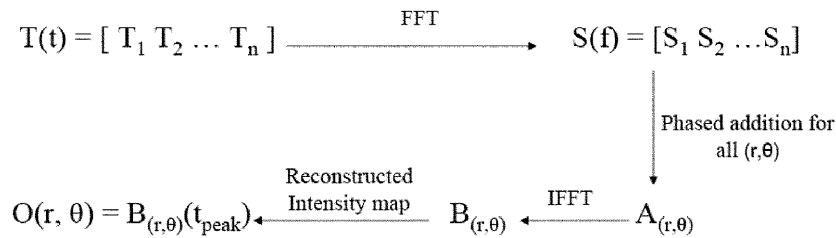
Fig. 3 A flowchart of the analysis procedure

transmitter to the imaging point, instead of the circular arc projection on the radial line. Referring to Fig. 2, the distance DR_i is approximated as equal to DB instead of DA. This approximation allows the simultaneous computation of intensities along all points in the direction by allowing the beam to steer along that direction. This approximation is acceptable for imaging defects that are located at large distances from the compact array, where the error of the approximation is minimal. The error in reconstruction is dependent on the r/D ratio (where r is the radial distance of the defect from the centre of the array) and this must be at least 3-4 for obtaining an acceptable level of reconstruction. The migration based reconstruction algorithm employs reconstruction for every point in the reconstruction domain, and hence the exact distances (for instance in the above case DR_i was used instead of DB) are used. In this case, the "near-field" limitation is overcome and this formulation of imaging can be applied for mapping reflector positions even when they are very close to the array.

4. Simulations for isotropic media

The features of the algorithm are brought out using the following simulation studies. A STMR system, consisting of a transmitter at the centre and 30 receivers equi-angularly spaced on the circumference of a circle of 12 cm diameter was considered placed on a 2 mm thick Al plate (isotropic plate) with infinite planar dimensions. The transducers were taken to operate at a frequency of 250 KHz and a tone burst, with a center frequency of 250 KHz and duration of 8 microseconds, was used for exciting the transmitter. The transducers are taken to be point elements. Ideal point defects were assumed for the simulation which scatters the signal uniformly to all the receivers. For reconstruction it is required that the defect should have at least one face normal to the radial direction so that the reflected signal from the defect can be captured by the receivers. Otherwise the received signal may be weak and thereby indistinguishable from the noise. Generally when the material properties and thickness are known a priori, an appropriate low frequency region is selected for excitation so that the number of modes present is minimal. The S_0 mode is chosen for excitation for the simulation studies. The dispersion plot for an Al plate of 2 mm thick is shown in the Fig. 4 along with the bandwidth of the PZT crystal that was used to excite the S0 guided Lamb mode in the plate. The dispersion curve data for the specific mode that was excited was used and the received signals at the various receiver locations
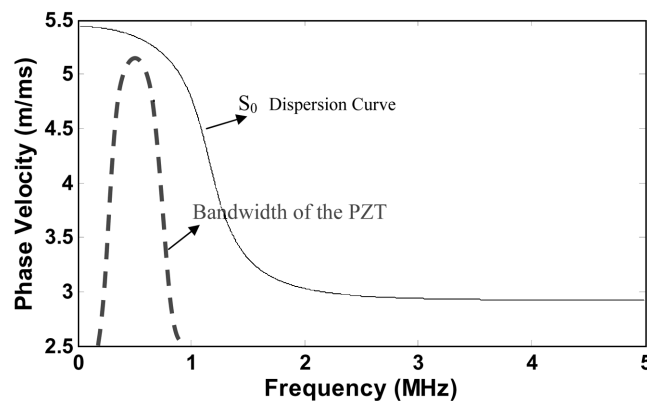

Fig. 4 The dispersion curve for the S_0 mode that was used in the simulation and experiments with the frequency bandwidth of the guided wave generated

were simulated and the phased addition algorithms (both the previously reported "far-field" and the migration based "near-field" algorithms) were used for generating the final reconstructed images.

The signals for simulations were simulated using the following method. For each defect, given the defect position, the total distance traveled by the excited wave to reach each receiver was calculated. Then, the dispersion curve data of the mode of interest was used to shift the frequency components of the transmitted signal spectra appropriately and then the simulated received signals at each receiver was computed. Let P denote the spectra of the pulse that is used to excite the Transmitter. Then the spectra of the received signal at j^{th} receiver (Q_j) as a function of frequency f is given by

$$Q_j(f) = P(f) \times \exp(-i2\pi f t_j) \tag{4}$$

where t_j is the time taken by the signal to travel from transmitter to the defect and then back to the receiver which is same as the time calculated in Eq. (2). Q_j is then subjected to an Inverse Fast Fourier Transform to obtain the time domain data representing the signals received at the receiver j. These signals, arranged column-wise with each column representing the signal received by a receiver, constitute the **T** matrix which is subjected to future processing and plotting as outlined above. In the image obtained, the origin (0,0) of all the plots are the location of the centre of the STMR compact array that is indicated by the black circle. The reconstructed image is then plotted in a dB scale normalized with the highest intensity in the image that is indicated at 0 dB that is represented by the black regions (which are expected to be the location of the defects or geometrical reflectors). The weakly reconstructed signals are lighter in the grey scale represents negative dB values compared to the reference signal maxima. Here, the signals of -20 dB and lesser were considered to be insignificant and hence are white. All of the reconstructed images were normalized to the peak signal value in the reconstructed image.

The 2 mm Al plate was assumed to have infinite lateral dimensions in order to avoid the complications of reflections from boundaries and corners. For the first simulation, defects were assumed at a distance of 0.4 m (defect 1) and 0.25 m (defect 2) from the array centre at angles of 0 and 90 degrees respectively
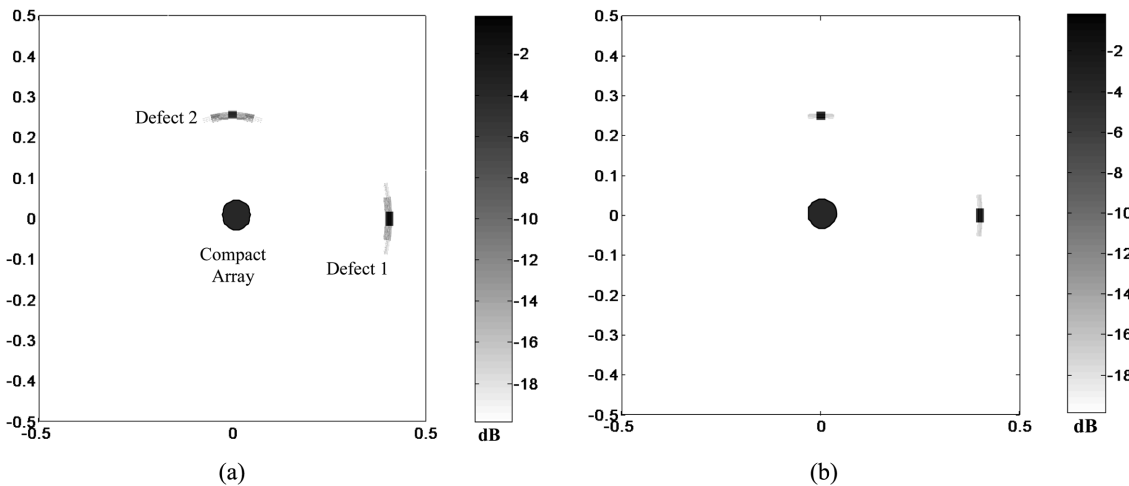

Fig. 5 Image obtained using simulated reconstruction of defects on 2 mm thick Al plate with 2 defects simulated at 0.40 m (along 0 deg) and 0.25 m (along 90) using (a) "far-field" approximation, and (b) the "near-field" corrected migration algorithm
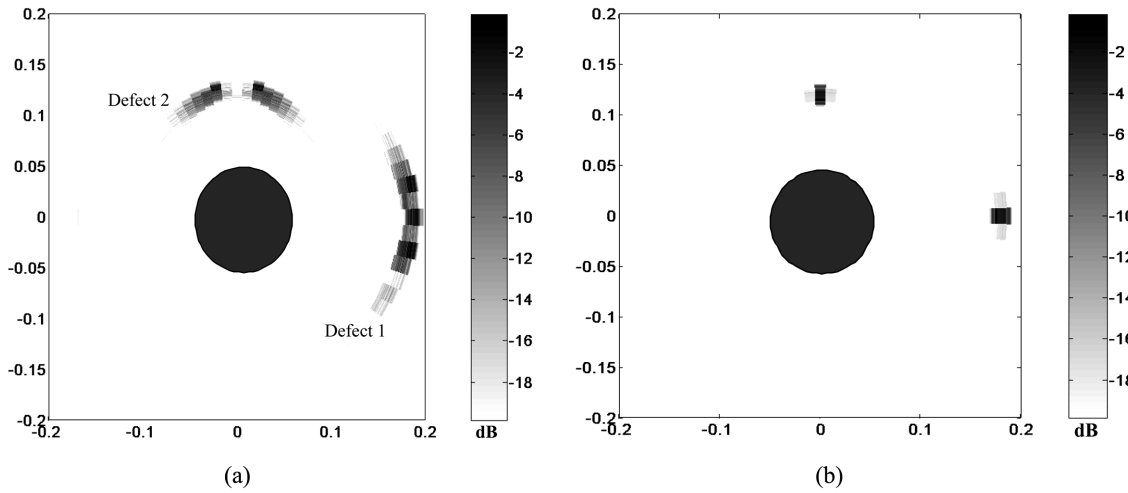
Fig. 6 Image obtained from simulated reconstruction of defects at 0.18 m (along 0 deg) and 0.12 m (along 90) using the (a) "far-field" approximation, and (b) migration algorithm

and signals are simulated. For comparison, the same is imaged using the "far-field" algorithm in Fig. 5(a) and using the migration based "near-field" corrected algorithm in Fig. 5(b). In Fig. 5(a), the defect at 0.4 m is slightly obscured whereas the image at 0.25 m is seen to blur extensively, and produce a broadening effect, as well as effects of side lobes are observed in the "far-field" algorithm reconstructed image. However the defects are accurately imaged in the case of the corrected migration based algorithm that is shown in Fig. 5(b). No side lobe effects were observed within the threshold level.

In the second simulation, defects were placed much closer to the compact array, at 0.18 m (defect 1) and 0.12 m (defect 2) radial distance from the array centre at angles of 0 and 90 degrees respectively. The result of the reconstruction is shown in Fig. 6. The improvement in the imaging of the defects that are present in the "near-field" corrected algorithm is clearly brought out with this case. The "far-field" algorithm shows a defect position angularly incorrect. It is found that the radial position was also incorrectly reconstructed because of this approximation, which will clearly observed when operating at higher frequency of excitation. The errors in the reconstruction increases as defects/reflectors get closer to the STMR compact array. This is understandable as the path corrections employed in the "far-field" case become less agreeable with the actual path corrections as the reflector comes closer to the array.

The computational intensity of the proposed algorithm was compared with the previous "far-field" algorithm using data from another simulation. The same array was used to obtain defect signals from a defect located at 40 cm from the centre of the array. The number of reconstruction angles chosen was 72. The computations were performed in a 3.0 GHz Pentium 4 computer with 1 GB Ram. The programming software used was MATLAB. The "far-field" algorithm finished the reconstruction in 3 seconds while the reconstruction using the "near-field" algorithm took 89 seconds. This marked difference is understandable as the "near-field" algorithm performs computations point by point over the whole domain, while the far field algorithm performs common computations for all radii along a particular angle, thereby reducing the time for reconstruction.

In all the simulations and experiments carried out in this paper, the defects have been assumed to be outside the compact array. The algorithm is not designed for imaging a defect that lies within the
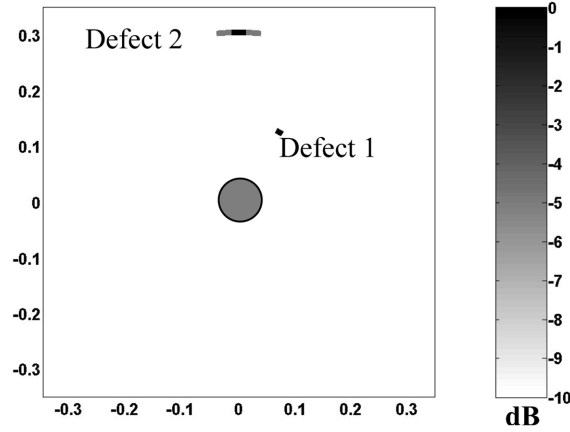
Fig. 7 Image obtained from simulated reconstruction of defects at 0.14 m (along 60 deg) and 0.3 m (along 90) using the migration algorithm

compact array, because the signal from the defect is observed to merge with the signals directly received from the transmitter, which are usually higher in amplitude. It is not possible to reliably time-gate the direct signals from defect reflected signals in this case, and can give rise to false alarms in the reconstruction.

5. Simulation for anisotropic media

Simulations were also performed in anisotropic media. The plate was taken to be 3.15 mm thick, with 21 layers. The first seven layers had fiber orientation of +45, -45, 0, 90, 0, -45, +45 degrees respectively which was repeated for the next 14 layers. The material properties were chosen to be Quasi- Isotropic. Defect 1 was placed at 0.14 m at an orientation of 60 deg and defect 2 was placed at 0.3 m at an orientation of 90 deg. The simulated signals were reconstructed and the result is shown in Fig. 7.

6. Performance study of STMR array

The STMR array system was subjected to a parameter study to determine the characteristics of the array. The simulations were carried out as described before for a 2 mm thick Al plate (isotropic).

6.1. Effect of inter-element spacing (Number of receivers for a given radius)

The simulations were carried out for array radius of 40 mm and excitation frequency of 250 kHz . The defect was located at a distance of 50 cm from the centre. The inter-element spacing was varied by changing the number of receivers. It is found that there is no change in both lateral as well as angular resolution if the number of receiver elements is increased. However there is a maximum inter-elemental spacing that is required to prevent the occurrence of grating lobes. It is safe to consider this maximum distance as to be equal to $\lambda_{min}/2$ where λ_{min} is the minimum wavelength present in the excited signal. Generally the grating lobes are not quite severe when this limit is slightly exceeded, and they are found
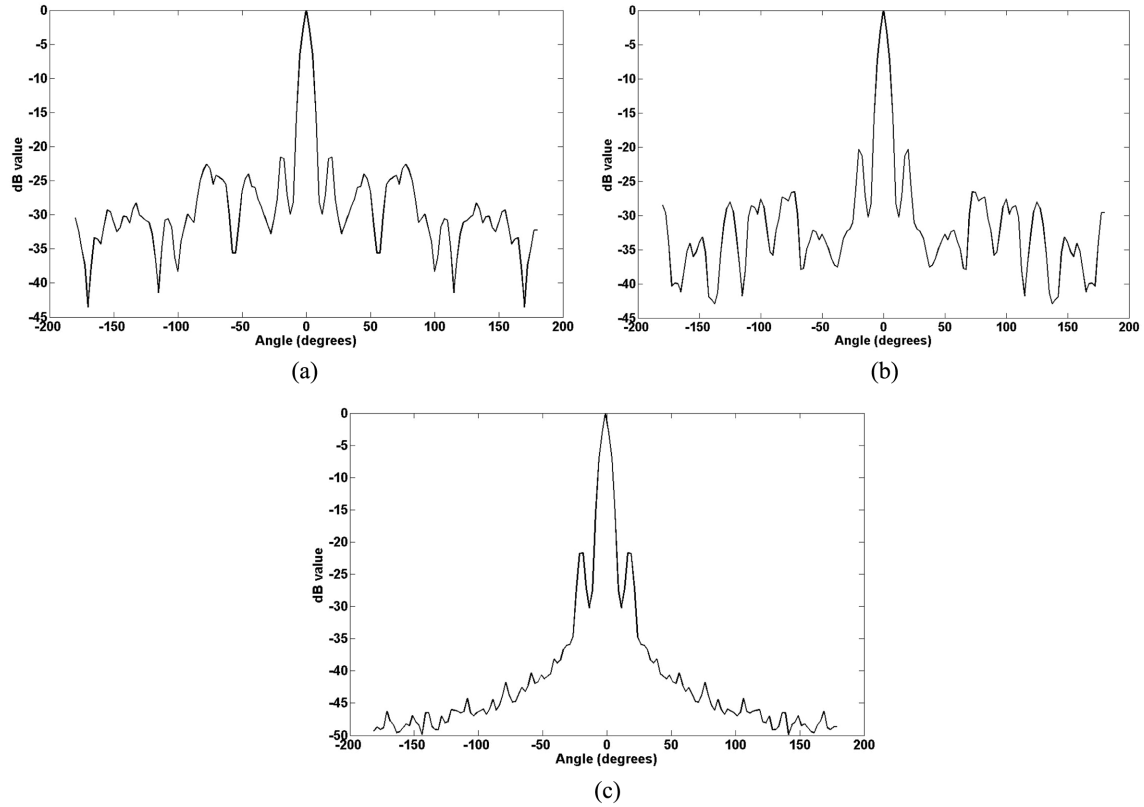
Fig. 8 PSF of a defect at 0.5m and 0 degrees using an array of radius 4 cm and (a) 10 receivers, (b) 18 receivers, (c) 26 receivers. Note the decrease of grating lobes as the number of receivers is increased

to have less pronounced effect which can be eliminated by proper threshold. Fig. 8 shows the variation of the Point Spread Function (PSF) of a point defect as the number of receivers is varied. It is observed that the severity of the grating lobes is decreased as number of receivers increases, whereas the main lobe and side lobe does not vary. Thus increasing the number of receiver elements does not lead to an improvement in resolution but there is a minimum number of elements needed to supress grating lobes. Also, effective threshold for imaging without false calls can be determined based on inter-element spacing. It is to be noted that the maximum inter-element spacing criteria indirectly limits the frequency of operation. As the size of an element is cannot be made very small, there is a minimum limit on the inter element spacing which is unavoidable. And for this, the maximum frequency of operation gets fixed because this maximum frequency determines the minimum wavelength. This limits the resolution obtained from the array, which increases with increase in frequency.

6.2. Radius of the STMR compact array

The radius of the array is varied from 10 mm to 65 mm and the results are shown in Fig. 9. The defect was placed at a distance of 50cm from the centre of the array. The grating lobe criterion is adhered to in all these simulations. The angular resolution increases with the increase in diameter. However radial resolution practically remains constant as diameter is increased. Thus an array with a larger diameter is
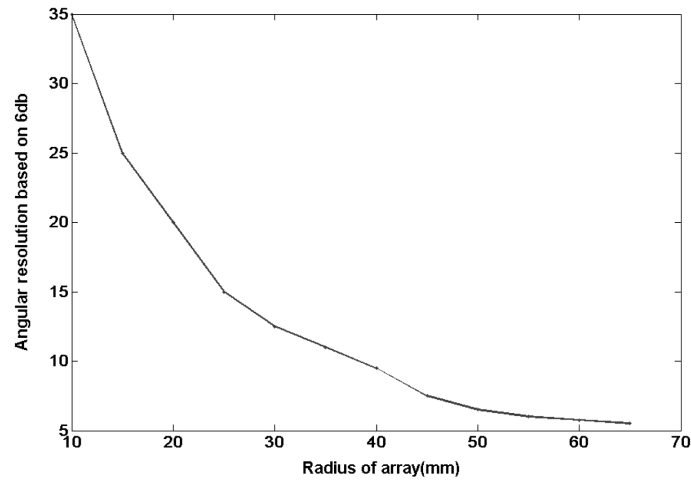
Fig. 9 Variation of angular resolution with radius of the array

preferred for obtaining better angular resolution. Also it was noted that angular resolution change with increase in the radius of the array follows exponential-like decay, whereas the effect is not pronounced if the array diameter is increased beyond a point. Note that this increase of radius however increases the "near-field" zone which cannot be imaged properly by the "far-field" algorithm. Thus by default, when one chooses to go for a larger diameter for obtaining better resolution, the near field algorithm is the only way out to minimize the zone of improper imaging.

7. Experiments

Experiments were performed on an Aluminum plate of 2 mm thickness. A Matec Instruments PR5000 Pulser/Receiver was used for exciting the transmitter and receiving the signals. A 20 MHz. Analog-Digital Converter (National Instruments USB 5102) was used for digital signal acquisition. The signals were sampled at 5 MHz and filtered after acquisition using a band pass filter so that high frequency noise and undesirable low frequency components were eliminated. The S_0 mode was used for reconstruction since this was the fastest mode and hence could be gated. The slower modes are often superimposed with the various reflections and hence cannot be reliably time gated.

In Fig. 10(a), which was obtained by migration based "near-field" reconstruction, the plate was defect free and only the edges of an 0.75 m by 0.75 m Al plate of thickness 2 mm was imaged. The transmitter, positioned at the center of the STMR compact array circle diameter of 160 mm, was excited with a sinusoidal input signal of center frequency 500 kHz. The receivers were kept at 24 equiangular spaced locations and the signals were obtained at these locations. Note that in this case the ratio of inter-element spacing to central frequency wavelength is 2. As explained before because of proper threshold, we see that the grating lobes are less visible in the reconstructed image.

In Fig. 10(b), the image of the plate was reconstructed after a circular defect of diameter 10 mm was introduced in the plate. Other parameters are kept the same. Both the edges of the plate as well as the defects are imaged. It is seen that in this case, during reconstruction the grating lobes are seen because the threshold of the image is increased in order to capture the location of the defect.

In Fig. 10(c), the same defect is imaged from a different location of the array. Also the frequency of
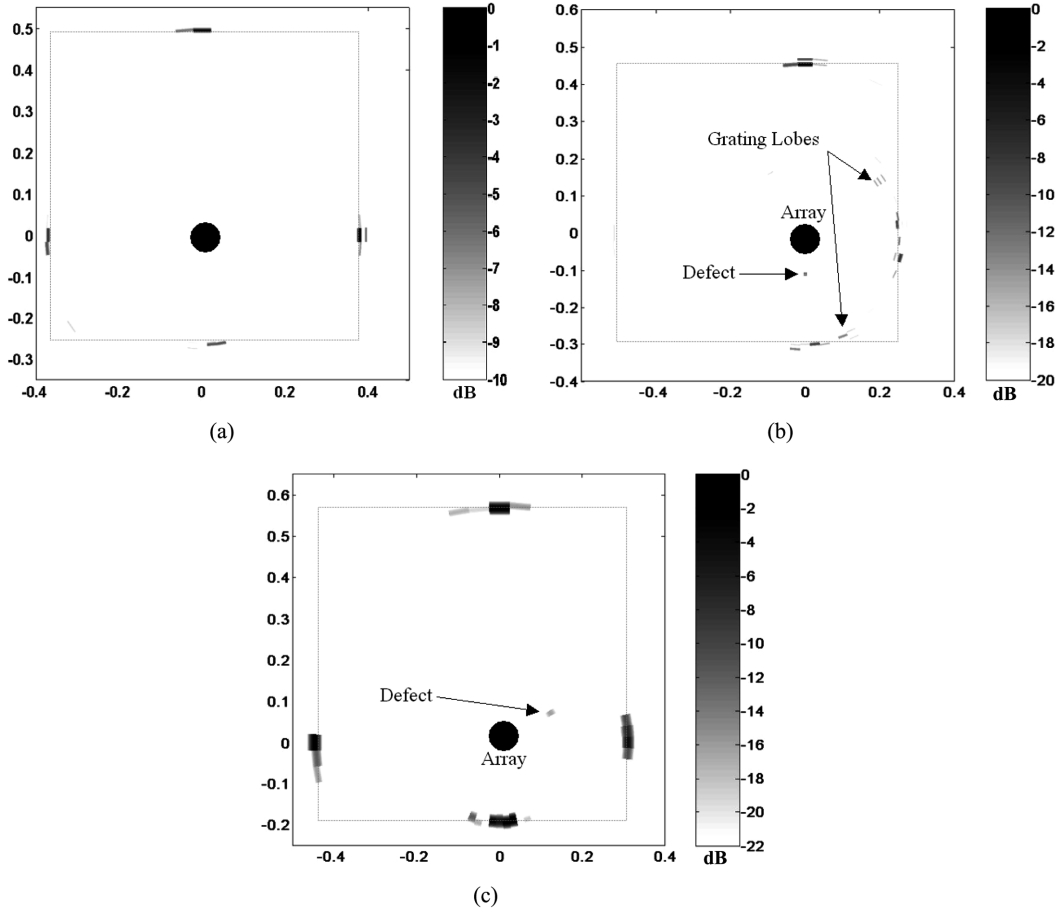
Fig. 10 Experimental results from the compact array on (a) defect free sample, (b) with defect, (c) with defect. The edge of the plate is also imaged well

operation was reduced to 200 kHz. The diameter of the array was reduced to 120 mm, and the number of receivers was increased to 36. Here, the grating lobe criterion is strictly satisfied as the ratio of spacing to wavelength corresponding to central frequency is '0.4'. It can be observed from the reconstructed image that the grating lobes were not seen. However, there is a significant decrease in quality of reconstruction (with respect to resolution) because of the lower frequency of operation. Thus while imaging defects and other weak reflectors, it is advised to adhere to the grating lobe criteria in order to image the features without false alarms, but at the expense of decreased resolution.

Another way to avert these grating lobes while reconstructing is suggested below. In the case of actual structural health monitoring (SHM) process, the array will consist of elements fixed on to the surface and hence one can get initial baseline data which contains information of geometrical reflectors such as edges and corners (which have a relatively large amplitude compared to the defect signals). The defect data can be obtained by normalizing the defective plate data from the non defective plate data. These processed signals when imaged, can be threshold appropriately so that the grating lobes can be avoided. Though this has not been dealt here, it has been shown possible

(Rajagopalan, *et al*. 2006).

8. Summary

In this paper, a new algorithm for imaging defects in a plate has been demonstrated to provide improved imaging in regions closer to the STMR array compared to the earlier reported beam-steering phase reconstruction algorithm. Simulations were performed and the results were compared with the conventional algorithm to highlight the advantages. The parameter study conducted provided the data reconstruction parameters that are optimal for the STMR array. It was found that the resolution increases as the diameter of the array increases and so the need for the near field corrected algorithm was also reinforced. Finally illustrative experiments were conducted highlighting the general aspects of imaging as well as proving the applicability of algorithm for reconstructing defects closer to the array.

The effect of side lobes during the reconstruction was also found to reduce significantly. A slight improvement was observed in both the simulated and experimental results in the "far-field" whereas the improvement in the "near-field" was significant. The migration reconstruction technique is slightly more computationally intensive, when compared to the previously reported approach. The polar coordinate based discretization was employed in the reconstructions presented in this paper. This leads to smaller grid sizes near the array and larger grid sizes at larger distances from the array. In order to avoid this, a Cartesian system of discretization may be also employed without any significant change in the reconstruction algorithm. It is to be noted that this modification cannot be carried out for the "far field algorithm which is designed for the polar coordinate system. It is expected that the Cartesian system based discretisation would have uniform grid sizes, but more number of discrete points to compute when compared to the polar discretization.

The long term strategy for the implementation of the STMR compact array in an aircraft SHM would either be a permanently attached patch on the skin of the structure or an embedded patch inside the skin, if the structure is a composite (Lin and Chang 2002, Giurgiutiu, *et al*. 2002). The embedment may be necessary for components where attachment is not permitted either due to presence of combustibles or other reasons. However, the limitation of the embedment of the sensor array would be the difficulty in repairing/replacing faulty sensors during the service life of the component/structure. The use of hybrid sensing methods including the use of fiber optics as receivers (Qing, *et al*. 2005) will result in further reducing the foot print of the compact array.

Some of the additional benefits of the proposed STMR compact array technique includes (a) The method is tolerant to slight errors in the positioning of receivers and the transmitter with respect to each other, (b) Materials like PVDF film sensors (which have good reception capabilities but poor transduction capabilities) can be used as receivers in an STMR system along with a PZT transmitter. This will result in a much lighter array system, which is critical for aerospace applications, (c) The technique can be extended to anisotropic plates, (d) the system can also be designed to be self-calibrating by using the initial signal received by the receivers to measure the material properties that can then be used in the phased addition reconstruction algorithm, (e) depending on the type of structure to be monitored other configurations such as semi-circular, elliptical, rectangular arrays etc. (Norton 2002) may be used in order to improve the performance of the algorithm.

The STMR compact array SHM technique is sensitive to reflectors in the plate and relatively in-sensitive to changes in the boundary conditions. This is an advantage if the array is used to monitor for

structural damage such as impacts and cracks since the technique is robust to external effects such as surface loading. However, the boundary conditions changes such as presence of liquids or adhesives will lead to leakage of the waves and thereby reducing the range of the monitoring system.

Acknowledgement

References

Bleistein, N. and Gray, S. H. (2001) "From the Hagedoorn imaging technique to Kirchhoff migration and inversion", *Geophysical Prospecting*, **49**, 629-43.

Boller, C. (2000), "Next generation structural health monitoring and its integration into aircraft design", *Int. J. Syst. Sci.*, **31**, 1333-1349.

Davies, J. and Cawley, P. (2006), "The application of synthetically focused imaging techniques for high resolution guided wave pipe inspection", *Proc. of the NDT 2006 - The 45th Annual British Conference on NDT*, 12-14 September, Stratford-upon-Avon, England, UK.

Fehler, M. C. and Huang, L. (2002), "Modern imaging using seismic reflection data", *Annu. Rev. Earth. Planet Sci.*, **30**, 259-284.

Fujino, Y. and Abe, M. (2004), "Structural health monitoring—current status and future", *Proceedings of 2nd European Workshop on Structural Health Monitoring*, Munich, Germany, 3-10.

Giurgiutiu, V. and Zagrai, A. (2002), "Embedded self-sensing piezoelectric active sensors for on-line structural identification", *ASME J. Vib. Acoust.*, **124**, 116-125.

Giurgiutiu, V., Zagrai, A. and Bao, J. (2002), "Embedded active in-situ structural monitoring of structures", *J. Pressure Vessel Technol.*, **124**, 293-99.

Jagannathan, R., Somasekhar, B. V., Balasubramaniam, K. and Krishnamurthy, C. V. (2004), "Plate waves structural health monitoring of composite structures", *Review of Progress in Quantitative Non-Destructive Evaluation*, **24B**, 1802-1808.

Lin, M. and Chang, F. K. (2002), "The manufacturing of composite structures with a built-in network of piezoceramics", *Comput. Sci. Technol.*, **62**, 919-39.

Malyarenko, E. V. and Hinders, M. K. (2001), "Lamb wave diffraction tomography", *Ultrasonics*, **39**, 269-81.

Norton, S. J. (2002), "Synthetic aperture imaging with arrays of arbitrary shape-Part I: General case", *IEEE Trans. Ultrason. Ferroelectr. Freq. Control*, **49**(4), 399-403.

Prasad, S. M., Balasubramaniam, K. and Krishnamurthy, C. V. (2003), "Structural health monitoring of composite structures using lamb wave tomography", *Smart Mater. Struct.*, **13**, N73-N79.

Prasad, S. M., Jagannathan, R., Balasubramaniam, K. and Krishnamurthy, C. V. (2003), "Structural health monitoring of anisotropic layered composite plates using guided ultrasonic lamb wave data", *Review of Progress in Quantitative Nondestructive Evaluation*, **23B**, 1460-67.

Prine, D. W. (1972), "Synthetic aperture ultrasonic imaging", *Proceedings of Engineering Applications of Holography Symposium, Society of Photo-optical Instrumentation Engineers*, Los Angeles, CA, USA, 287.

Qing, X., Kumar, A. Zhang, C., Gonzalez, I. and Chang, Fu-Kuo (2005), "High speed hybrid piezoelectric/fiber optic diagnostic system for structural health monitoring", *Smart Mater. Struct.*, **14**(3), S98-103.

Rajagopalan, J., Balasubramaniam, K. and Krishnamurthy, C. V. (2006), "A single transmitter multi receiver (STMR) PZT array for guided ultrasonic wave based structural health monitoring of large isotropic plate structures", *Smart Mater. Struct.* **15** 1190-1196.

Rajagopalan, J., Balasubramaniam, K. and Krishnamurthy, C. V. (2006) ,"A phase reconstruction algorithm for Lamb wave based structural health monitoring of anisotropic multilayered composite plates", *J. Acoust. Soc.*

Am., **119**(2), 872-878.

Rose, J. L. (1999), *Ultrasonic Waves in Solid Media*, Cambridge University Press.

Sicard, R., Goyette, J. and Zellouf, D. (2002), "A SAFT algorithm for lamb wave imaging of isotropic plate-like structures", *Ultrasonics*, **39**, 487-94.

Schmitz, V., Chakhlov, S. and Muller, W. (2000), "Experiences with synthetic aperture focusing technique in the field", *Ultrasonics*, **38**, 731-38.

Seydel, J. (1982), "Ultrasonic synthetic aperture focusing techniques in NDT", Research Techniques in Non destructive Testing(Academic Press), **VI**, 1-47.

Sicard, R., Goyette, J. and Zellouf, D. (2002), "A numerical dispersion compensation technique for time recompression of Lamb wave signals", *Ultrasonics*, **20**, 727-732.

Spies, M. and Jager, W. (2003), "Synthetic aperture focusing for defect reconstruction in anisotropic media", *Ultrasonics*, **41**, 125-131.

Subbarao, P. M. V., Munshi, P. and Muralidhar, K. (1996) "Performance of iterative tomographic algorithms applied to non-destructive evaluation with limited data", *NDT&E*, **30**(6), 359-70.

Victorov, I. (1967), *Rayleigh and Lamb Waves: Physical Theory and Applications*, Plenum Press, New York.

Wilcox, P. D., Lowe, M. and Cawley, P. (1999), "Lamb and SH wave transducer arrays for the inspection of large areas of thick plates", *Review of Progress in Quantitative Non-Destructive Evaluation*, **19A**, 1049-56.

Wilcox, P. D., Lowe, M. J. S. and Cawley, P. (2000), "A signal processing technique to remove the effect of dispersion from guided wave signals", *Review of Progress in Quantitative Non-Destructive Evaluation*, **20A**, 555-562.

Wilcox, P. D. (2002), "Guided wave beam steering from omni-directional transducer arrays", *Review of Progress in Quantitative Non-Destructive Evaluation*, **22A**, 761-68.

Wilcox, P. D. (2003), "Omni-directional guided wave transducer arrays for the rapid inspection of large areas of plate structures", *IEEE Transactions on Ultrasonics, Ferroelectrics and Frequency Control*, **50**(6), 699-709.

JK